6th European Conference on Computational Mechanics (ECCM 6)
7th European Conference on Computational Fluid Dynamics (ECFD 7)
11–15 June 2018, Glasgow, UK

NUMERICAL SIMULATION OF A PARTICLE TRANSPORT IN THE FLAT CHANNEL

DMITRIY KURANAKOV[1], DENIS ESIPOV[1], VASILIY LAPIN[1] AND LEONID ANISYUTIN[1]

[1] Institute of Computational Technologies SB RAS
6 Academician M.A. Lavrentiev avenue, Novosibirsk, 630090, Russia
kuranakov@ict.sbras.ru

Key words: Immersed Boundary Method, fluid-particle interaction, Segre-Silberberg effect

Abstract. The problem of the proppant transport, sedimention and jamming in the hydraulic fracture is of current scientific and technological interest. For fully resolved simulations of these processes a new model of incompressible viscous fluid flow with the immersed solid particles is presented. The fluid-particle interaction is modeled using the Immersed Boundary Method (IBM). For better approximation of the no-slip boundary condition the multidirect forcing scheme is applied that consists in iterative correction of the applied force. Particle transfer and rotation are simulated using the Newton-Euler equations. The main feature of the proposed model is fully coupling of the fluid velocity and the particle velocity using iterations. The proposed model was verified using the benchmark problems: cavity flow problem, flow around the cylinder, the transfer and rotation of a single particle in Poisseuille flow (Segre-Silberberg effect). The problem was solved for various Reynolds numbers, particle sizes, densities, starting positions and shapes.

1 INTRODUCTION

Many problems in nature and engineering involve flows of mixture that consists of viscous fluid and particles of arbitrary sizes and shape. There are a few ways to simulate such flows.

When the size of the particles is small relative to the characteristic size of the fluid flow, the mixture is modeled as the "effective" viscous incompressible fluid. The rheology parameters of the effective fluid are functions of the particles concentration.

But if the particle size is comparable with the characteristic size of the flow, one have to consider each particle separately. In that way the direct numerical simulation (DNS) is used. In this approach the hydrodynamic interactions between fluid and particles, particles and walls as well as between particles themselves are simulated without any averaging. Fluid is described in scope of Navier–Stokes (NS) equations. The particles are

not treated as a phase but movement of each one is considered using the Newton-Euler equations.

DNS methods can be divided into two main groups by the way how the wall and particle boundaries are described by the computational mesh.

The methods of the first group such as Arbitrary Lagrangian–Eulerian method [1] use computational meshes that conform to the physical boundaries of the particles and the computational domain. In these methods boundary conditions are satisfied directly and don't reduce the order of the approximation of the whole problem. The another advantage is that the forces applied to the particles are obtained without any additional supposition. In this method the computational mesh is constructed at each time step to fit the boundaries of the particles that moves in accordance with Newton's law. On the other hand, in the case of a large number of particles the Arbitrary LagrangianEulerian method is less effective [2]. The main reason of that and the main drawback of the methods with accurate boundary representation is the complexity of the mesh generation procedure and projection errors caused by the remeshing that reduces the solution accuracy.

The problem of remeshing is common for all methods with accurate boundary description so the cases with many particles is preferably to simulate using computational meshes that do not fit the boundaries. Such methods are Fictitious Domain Method (FDM) [3–5] and the Immersed Boundary Method (IBM) [6]. These methods are based on the idea of solving the flow equation on a mesh, over the entire domain, and defining the objects inside the flow by adding Lagrangian points on their surfaces which may or may not coincide with the Eulerian grid. Methods without mesh rebuilding are characterized by simpler meshes, since it is not necessary to describe the domain boundaries.

In both groups of the methods the effect of particles on a fluid flow is described by the addition of forces to the equations of fluid motion. In FDM forces are added in the mesh cells, occupied by particles, such that the velocities inside the particle are equal to the velocity of the solid body. In the cells adjacent to the particle the forces are added such that the no slip condition at the fluid-particle boundary is satisfied. As it stated in [7] the main problem of fictitious boundary methods is low accuracy in approximating the boundaries through a non-adaptive grid.

The IBM proposed in [6] is based on the similar to FDM idea that the presence of the solid particle inside the fluid flow domain can be formulated by adding appropriate forces acting on the fluid. The difference is that in the IBM the forces are added in the vicinity of the boundary while in FDM the forces are added inside the particle. Many modifications and variant versions of IBM were developed to enhance accuracy, stability and range of applications.

As it stated in [8] the last decade has witnessed a great interest in the fully-resolved simulation of flows with many suspended particles. The majority of these studies use some variant of the IBM. One of the directions of IBM development is the improvement of its stability for wide range particle–fluid mass density ratio. Versions of the IBM proposed in [9–12] are applicable for particle–fluid mass density ratio form 0.3 to 1000 and demonstrate the second order of approximation.

We propose a variant of IBM method in which particle velocities, fluid velocities,

pressure and fluid-solid interaction forces are fully coupled in iterative scheme. For better approximation of the no-slip boundary condition the multidirect forcing scheme is applied that consists in iterative correction of the applied force.

2 GOVERNING EQUATIONS

We consider the problem of a viscous, incompressible fluid flow in a plane channel with an absolutely rigid body placed there. The fluid flow is governed by the Navier-Stokes equations

$$\begin{aligned} \rho\frac{d\,\mathbf{u}}{dt} &= \mu\Delta\,\mathbf{u} - \nabla p + \rho\,\mathbf{f}, \\ \nabla\cdot\mathbf{u} &= 0, \end{aligned} \tag{1}$$

where $\mathbf{u} = (u, v)^T$ is the velocity vector, p is the pressure, ρ is the fluid density, μ is the dynamic viscosity, $\mathbf{f}$ is the fictitious body force that affects the fluid flow near the surface of the immersed body, $\dfrac{d\,\mathbf{u}}{dt}$ means the total derivative

$$\frac{d\,\mathbf{u}}{dt} = \frac{\partial\,\mathbf{u}}{\partial t} + (\mathbf{u}\cdot\nabla)\,\mathbf{u}\,. \tag{2}$$

Hydrodynamic stress tensor $\boldsymbol{\sigma}$ with components σ_{ij} is written as follows

$$\sigma_{ij} = -\delta_{ij}p + \mu\dot{\varepsilon}_{ij}, \tag{3}$$

where $\dot{\varepsilon}_{ij}$ is the strain rate tensor.

In terms of stress tensor $\boldsymbol{\sigma}$ the Navier-Stokes equation is rewritten as follows

$$\rho\frac{d\,\mathbf{u}}{dt} = \nabla\,\boldsymbol{\sigma} + \rho\,\mathbf{f}\,. \tag{4}$$

The velocity $\mathbf{u}_p$ at each point of the absolutely rigid particle can be decomposed into the translational part and the rotational part

$$\mathbf{u}_p = \mathbf{u}_c + \boldsymbol{\omega}\times\mathbf{r}, \tag{5}$$

where $\mathbf{u}_c$ is the translational velocity of the particle centroid, $\boldsymbol{\omega}$ is the angular velocity of the particle. The motion of the single particle is described by the NewtonEuler equations for $\mathbf{u}_c$ and $\boldsymbol{\omega}$

$$\begin{aligned} \rho_p V_p\frac{d\,\mathbf{u}_c}{dt} &= \rho\int\limits_{\Gamma_p}(\boldsymbol{\sigma}\cdot\mathbf{n})d\Gamma = \rho\int\limits_{V_p}(\nabla\cdot\boldsymbol{\sigma})dV, \\ \rho_p I_p\frac{d\,\boldsymbol{\omega}}{dt} &= \rho\int\limits_{\Gamma_p}\left[\mathbf{r}\times(\boldsymbol{\sigma}\cdot\mathbf{n})\right]d\Gamma = \rho\int\limits_{V_p}\left[\mathbf{r}\times(\nabla\cdot\boldsymbol{\sigma})\right]dV. \end{aligned} \tag{6}$$

The particle is assumed to be homogeneous with density ρ_p, I_p is the moment of inertia of the particle with unit density, V_p is the volume of the particle with the surface $\Gamma_p = \partial V_p$, $\mathbf{n}$ is the outward-pointing unit normal in Γ_p, the stress tensor $\boldsymbol{\sigma}$ equals the one in Navier-Stokes equation (4).

In IBM the integrals in (6) are not calculated directly. The stress tensor $\nabla \cdot \boldsymbol{\sigma}$ is substituted from (4) into (6) and the following equations are considered

$$\begin{aligned} \rho_p V_p \frac{d\,\mathbf{u}_c}{dt} &= \rho \frac{d}{dt} \int\limits_{V_p} \mathbf{u}\, dV - \rho \int\limits_{V_p} \mathbf{f}\, dV, \\ \rho_p I_p \frac{d\,\boldsymbol{\omega}}{dt} &= \rho \frac{d}{dt} \int\limits_{V_p} [\mathbf{r} \times \mathbf{u}]\, dV - \rho \int\limits_{V_p} [\mathbf{r} \times \mathbf{f}]\, dV. \end{aligned} \tag{7}$$

In [13] it is assumed that the velocity of the fluid inside the solid particle satisfies the rigid body motion condition (23). Substituting (23) to (7), we obtain the motion equations for a single particle

$$\begin{aligned} \left(\frac{\rho_p}{\rho} - 1\right) V_p \frac{d\,\mathbf{u}_c}{dt} &= -\int\limits_{V_p} \mathbf{f}\, dV, \\ \left(\frac{\rho_p}{\rho} - 1\right) I_p \frac{d\,\boldsymbol{\omega}}{dt} &= -\int\limits_{V_p} [\mathbf{r} \times \mathbf{f}]\, dV. \end{aligned} \tag{8}$$

So the motion of the particle is calculated using only the force $\mathbf{f}$. In the case when the densities of the particles are close to each other, this method becomes unstable, and the direct calculation of the integrals of velocity change inside the particle is needed [9].

The model consists of fluid flow equations (1) and motion of particle equations (8).

3 NUMERICAL METHOD

3.1 Spatial discretization

Our method is based on the IBM developed in [13] and improved in [9]. This is a so-called direct forcing method in which the additional force $\mathbf{f}$ is applied separately after the discretization of Navier-Stokes equation.

The fluid flow is discretized using the Eulerian grid, and the solid body surface uses the Lagrangian grid Γ_p, as shown in fig. 1.

The quantities in Euler grid are denoted by lower case letters with index (i, j) $(\mathbf{x}_{ij}, \mathbf{u}_{ij}, \mathbf{f}_{ij})$. The Lagrangian quantities are denoted by upper case letters with index l $(\mathbf{X}_l, \mathbf{U}_l, \mathbf{F}_l)$. The transfer from Eulerian grid to Lagrangian one is performed using the regularized Delta function δ_d proposed by Griffith and Peskin [14]

$$\mathbf{U}_l = \mathbb{EL}(\mathbf{u}_{ij}) = \sum_{ij} \mathbf{u}_{ij}\, \delta_d(\mathbf{x}_{ij} - \mathbf{X}_l) h_x h_y. \tag{9}$$

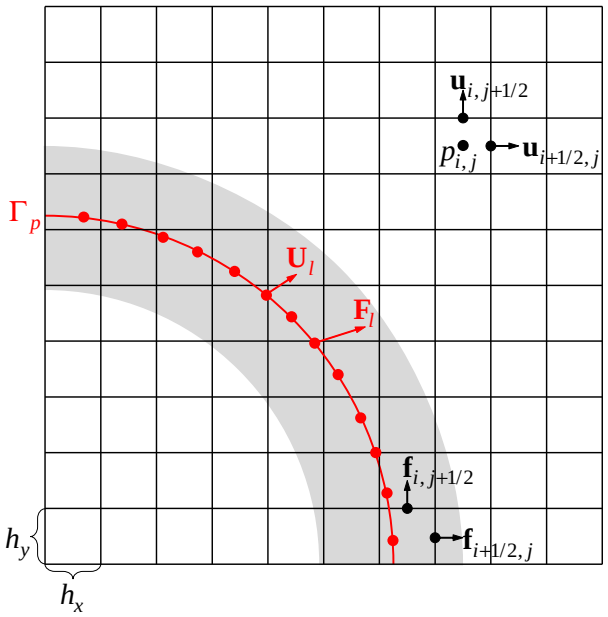

Figure 1: Lagrange and Euler meshes.

The inverse transfer from Lagrangian grid to Eulerian grid is made using formula

$$\mathbf{f}_{ij} = \mathbb{LE}(\mathbf{F}_l) = \sum_l \mathbf{F}_l \, \delta_d(\mathbf{x}_{ij} - \mathbf{X}_l)\Delta V_l. \tag{10}$$

Here h_x, h_y are the dimensions of the Eulerian grid and ΔV_l is the volume of the Lagrangian grid cells.

The non-slip boundary condition is applied in Lagrangian grid

$$\mathbf{U}_p(\mathbf{X}_l) = \mathbf{U}_l \, . \tag{11}$$

Here $\mathbf{U}_p(\mathbf{X}_l)$ is the velocity of the solid particle in the node $\mathbf{X}_l$ of Lagrangian grid, $\mathbf{U}_l$ is the fluid velocity in this node.

3.2 SIMPLE method for Navier-Stokes equations solution

At the new time step $n+1$ we predict the velocity of the fluid using the discretized Navier-Stokes equation

$$\frac{\mathbf{u}^{n+1} - \mathbf{u}^n}{\tau} + \frac{(\mathbf{u}\,\nabla\,\mathbf{u})^n + (\mathbf{u}\,\nabla\,\mathbf{u})^{n+1}}{2} = -\frac{\nabla p^{n+1/2}}{\rho} + \frac{1}{\mathrm{Re}}\frac{(\Delta\,\mathbf{u})^n + (\Delta\,\mathbf{u})^{n+1}}{2}. \tag{12}$$

The force term $\mathbf{f}$ is not included to equation (12) and is applied further while correcting the velocity. Equation (12) includes non-linear pressure gradient term and convection term. In that way the iterations s are introduced to find the unknown pressure $p^{s+1} = p^{n+1/2}$ and velocity $\mathbf{u}^{s+1} = \mathbf{u}^{n+1}$ distributions. At each iteration s the unknown velocity $\mathbf{u}^{s+1}$ is calculated in several steps using intermediate first ($\mathbf{u}^*$) and second ($\mathbf{u}^{**}$) prediction

velocities [9]. The initial values of velocity and pressure are taken from the previous time step: $s = 0$, $p^s = p^{n-1/2}$, $\mathbf{u}^s = \mathbf{u}^n$. The first prediction velocity $\mathbf{u}^*$ is calculated using Navier-Stokes equation for given pressure p^s

$$\frac{\mathbf{u}^* - \mathbf{u}^n}{\tau} + \frac{(\mathbf{u}\nabla\mathbf{u})^n + (\mathbf{u}\nabla\mathbf{u})^s}{2} = -\nabla p^s + \frac{1}{\mathrm{Re}}\frac{(\Delta\mathbf{u})^n + (\Delta\mathbf{u})^*}{2} \tag{13}$$

The system of non-linear equations arising due to the presence of non-linear term $(\mathbf{u}\nabla\mathbf{u})$ is solved by the Biconjugate gradient stabilized method (BiCGStab).

Then the force $\mathbf{f}$ acting from the particle to the fluid is applied and the second prediction velocity $\mathbf{u}^{**}$ is calculated

$$\mathbf{u}^{**} = \mathbf{u}^* + \tau\,\mathbf{f}\,. \tag{14}$$

The detailed description of force calculation will be presented further.

The correction of pressure $\tilde{p}$ is found from the Poisson equation with second prediction velocity $\mathbf{u}^{**}$.

$$\Delta\tilde{p} = \frac{\rho}{\tau}\nabla\cdot\mathbf{u}^{**}\,. \tag{15}$$

The solution of Poisson equation (15) is found using the Seidel iterative method.

Finally the pressure p^{s+1} and the velocity $\mathbf{u}^{s+1}$ are corrected and transition to the next iteration step s takes place

$$\begin{aligned} p^{s+1} &= p^s + \tilde{p}, \\ \mathbf{u}^{s+1} &= \mathbf{u}^{**} - \frac{\tau}{\rho}\nabla\tilde{p}. \end{aligned} \tag{16}$$

The iterations allow to fulfill the continuity equation with the given precision, even if the initial distribution of the pressure is far from the the required one.

3.3 Immersed boundary method. Direct and multidirect forcing schemes

The immersed boundary method consists in introducing the fictitious force $\mathbf{f}$ to the Navier-Stokes equation (1) in such a way that the fluid velocity at the surface of the particle satisfies the non-slip condition (11).

Direct forcing scheme consists in the following. The first prediction velocity is interpolated from Eulerian grid to Lagrangian grid using (9)

$$\mathbf{U}_l^* = \mathbb{EL}(\mathbf{u}_{ij}^*) \tag{17}$$

The force $\mathbf{F}_l$ in Lagrange nodes is corrected using the difference between the fluid first prediction velocity $\mathbf{U}_l^*$ and the solid particle velocity $U_s(\mathbf{X}_l)$

$$\mathbf{F}_l = \frac{\mathbf{U}_p(\mathbf{X}_l) - \mathbf{U}_l^*}{\tau}, \tag{18}$$

The force is interpolated to the Euler mesh

$$\mathbf{f}_{ij} = \mathbb{LE}(\mathbf{F}_l) \tag{19}$$

The force $\mathbf{f}_{ij}$ is applied to the first prediction velocity $\mathbf{u}^{*}_{ij}$ and the second prediction velocity $\mathbf{u}^{**}_{ij}$ is calculated

$$\mathbf{u}^{**}_{ij} = \mathbf{u}^{*}_{ij} + \tau\, \mathbf{f}_{ij}\,. \tag{20}$$

Using the regularized delta-function for the interpolation results in a diffuse distribution of the force around the interface of the particle. Therefore the calculated velocity $\mathbf{u}^{**}_{ij}$ satisfies the no-slip boundary condition (11) not very well.

In [15] the multidirect forcing scheme was proposed to improve the force and velocity calculation. In this method the force is applied and the second prediction velocity is corrected several (N_f) times. In the initial iteration $f = 0$ the value of second prediction velocity equals to the first prediction velocity $\mathbf{u}^{**,f}_{ij} = \mathbf{u}^{*}_{ij}$. Then the direct forcing scheme is applied N_f times

$$\begin{aligned}
&\mathbf{U}^{**,f}_{l} = \mathbb{EL}(\mathbf{u}^{**,f}_{ij}),\\
&\mathbf{F}^{f}_{l} = \frac{\mathbf{U}_p(\mathbf{X}_l) - \mathbf{U}^{**,f}_{l}}{\tau},\\
&\mathbf{f}^{f}_{ij} = \mathbb{LE}(\mathbf{F}^{f}_{l}),\\
&\mathbf{u}^{**,f+1}_{ij} = \mathbf{u}^{**,f}_{ij} + \tau\, \mathbf{f}^{f}_{ij}\,.
\end{aligned} \tag{21}$$

Finally the second prediction velocity is $\mathbf{u}^{**}_{ij} = \mathbf{u}^{**,N_f}_{ij}$, and the applied force is $\mathbf{f}_{ij} = \sum_{f=0}^{N_f} \mathbf{f}^{f}_{ij}$. The multidirect forcing scheme is used instead its simplified representation in equation (14).

4 NUMERICAL EXPERIMENTS

4.1 Stationary flow around the cylinder in large domain

For the verification of the method we solve the benchmark problem of the stationary flow around the cylinder placed to the infinite domain and compare it with the results obtained by other researchers. The cylinder diameter equals $D = 1$, the inflow velocity is $U = 1$. The domain is taken large enough to reduce the influence of the domain finiteness (15×15). The mesh sizes are 300×300. The cylinder is place closer to the inflow wall at distance 5 from it. The pressure distributions and streamtraces for two values of Reynolds number $\mathrm{Re} = 20$ and $\mathrm{Re} = 40$ are presented in fig. 2. Two symmetric vortices at the leeward sides of each cylinder are generated. The summary of results and comparison to other authors is presented in table 1. We compare the drag force coefficient $C_d = \dfrac{2f_d}{\rho U^2 D}$, the length L of recirculation zone and the angle θ of separation point. The values of the drag force and the size of the vortices behind the cylinder are overestimated. This may be caused by the diffuse distribution of the IBM force that increases the real size of the cylinder and the finite size of the domain as was mentioned in [13]. The streamlines pass very close to the cylinder that demonstrates that the no-slip boundary condition is fulfilled with high presision.

Table 1: Summary of the results and comparison to other investigators for Re = 20 and Re = 40.

	Re = 20			Re = 40		
	C_d	L	θ	C_d	L	θ
Fornberg (1980) [16]	2.0	0.91	43.2°	1.5	2.24	55.6°
Calhoun (2002) [17]	2.19	0.91	45.5°	1.62	2.18	54.2°
Russel and Wang (2003) [18]	2.02	0.93	43.2°	1.52	2.32	53.1°
Our method	2.4	1.06	38.5°	1.8	2.4	47.1°

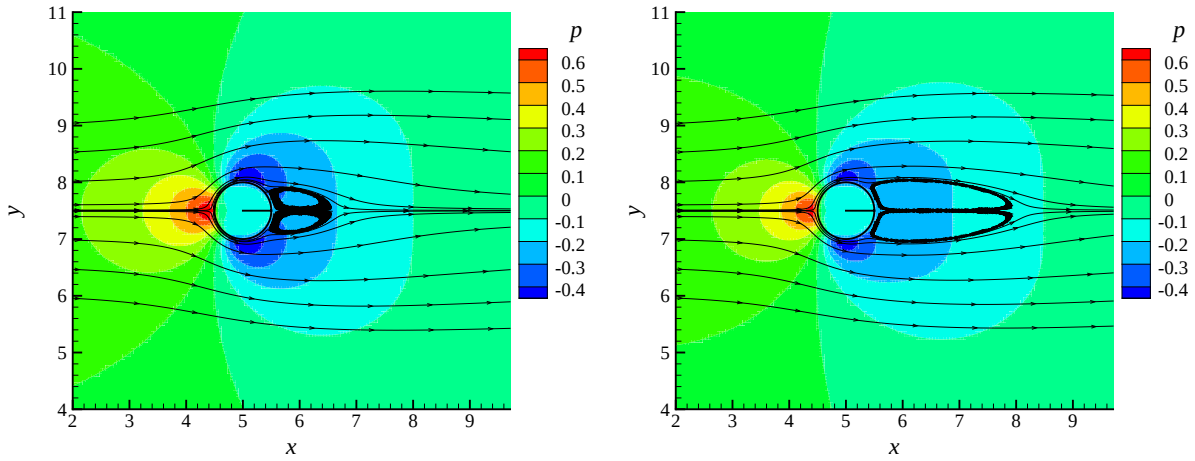

Figure 2: Pressure distribution and streamtraces for the flow around the cylinder problem with Re = 20 (left) and Re = 40 (right).

4.2 Non-stationary flow around the cylinder in large domain

In the case of Re = 100 the flow becomes unstable and the von Krmn vortex street develops. To verify our method we compare the drag force coefficient C_d and its oscillation amplitude, lift force C_l oscillation amplitude and the Strouhal number $St = \dfrac{d}{UT}$. The results are presented in table 2.

Table 2: Summary of the results and comparison to other investigators for Re = 100.

	C_d	C_l	St
Xu and Wang (2006) [19]	1.42 ± 0.013	± 0.34	0.171
Calhoun (2002) [17]	1.33 ± 0.014	± 0.298	0.175
Russell (2003) [18]	1.38 ± 0.007	± 0.276	0.165
Our method	1.53 ± 0.011	± 0.376	0.170

The evolution of C_d and C_l is shown in fig. 3. While the von Krmn vortex street is not formed yet the drag C_d falls down the value of 1.29 and the lift C_l equals zero. Then the von Krmn vortices start to separate from the surface of the cylinder and the drag force increases to the value of 1.53. The oscillation amplitudes of drag and lift are 0.011

and 0.376 correspondingly. As in the case of stationary flow the values of the forces are overestimated due to the diffusion of IBM force. The snapshots of pressure distribution and streamtraces for one period T of oscillation are shown in fig. 4.

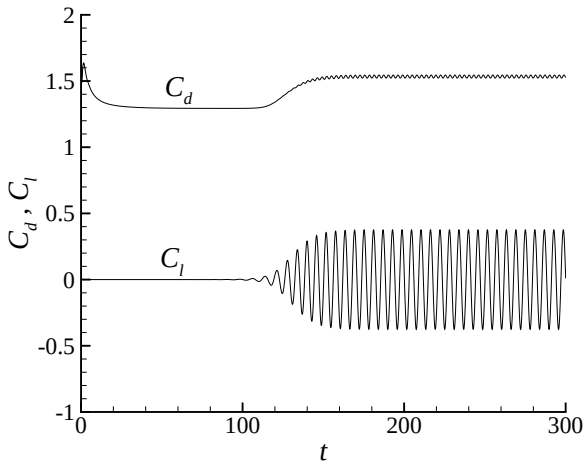

Figure 3: Drag C_d and lift C_l forces versus time t for the flow around the cylinder with $\mathrm{Re} = 100$.

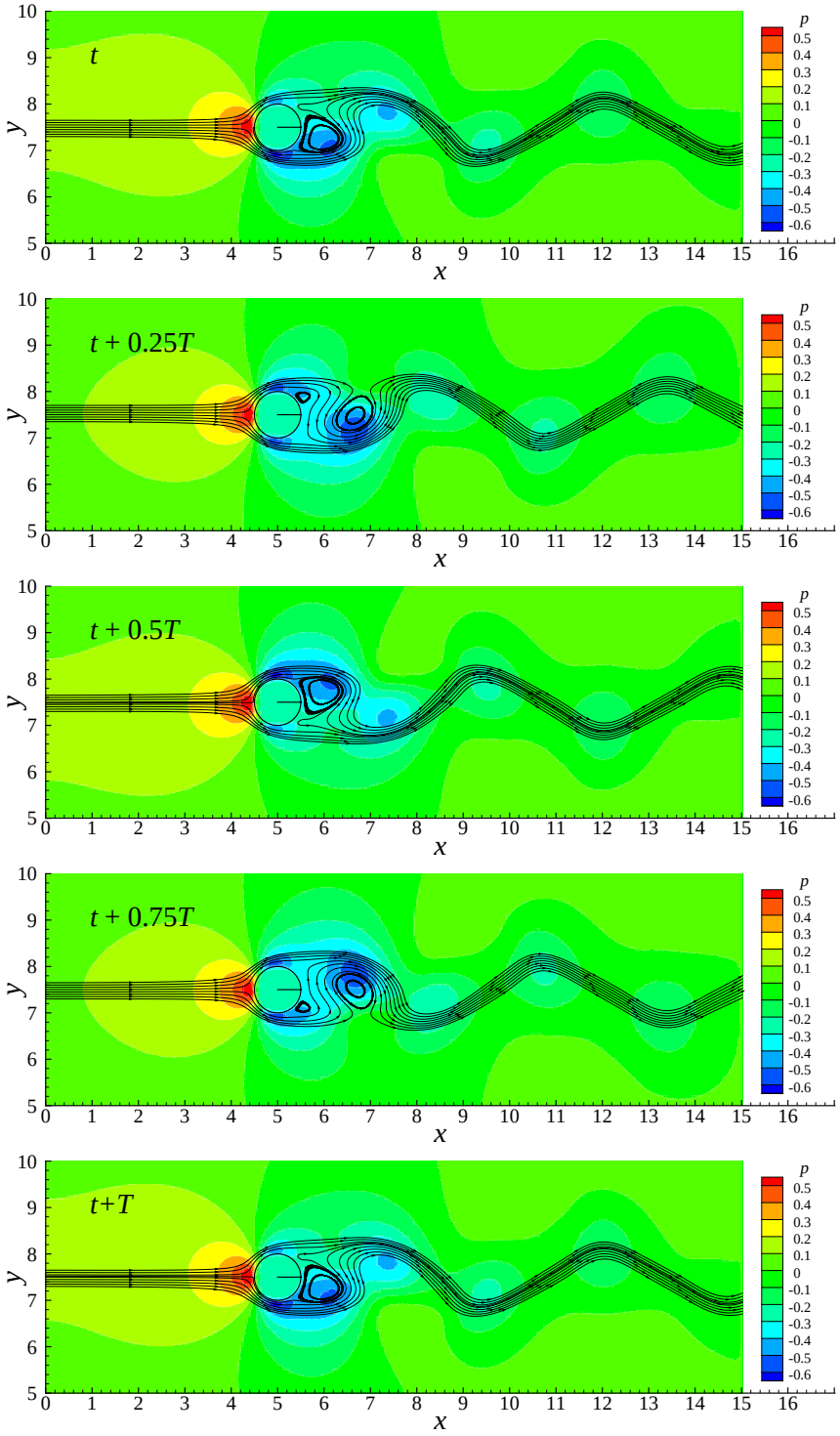

Figure 4: Pressure distribution and streamtraces for the flow around the cylinder problem with Re = 100 for one period T of oscillation.

4.3 Poiseuille flow with one particle

The flow configuration is illustrated in fig. 5. The solid round particle of diameter D is placed into a periodical channel of width W and length L.

The initial distribution of fluid velocity are given by the undisturbed Poiseuille fluid flow with maximal velocity $u_0 = 1$:

$$u(x, y) = u_0 = 1 - \left(\frac{y - W/2}{W/2}\right)^2. \tag{22}$$

The initial translational u_c and rotational ω velocities of the particle are given by the undisturbed Poiseuille fluid flow:

$$u_c(x, y) = u_0, \quad \omega(x, y) = \frac{1}{2}\frac{\partial u_0}{\partial y} = \frac{y - W/2}{(W/2)^2}. \tag{23}$$

At the channel boundaries and in the surface of the immersed solid particles no-slip boundary conditions are applied

$$\mathbf{u}\Big|_{\Gamma_w} = 0, \quad \mathbf{u}\Big|_{\Gamma_p} = \mathbf{u}_p\,. \tag{24}$$

The difference of the pressure between the inlet and outlet of the channel corresponding to the Poisseuille flow is applied

$$p\Big|_{\Gamma_{in}} - p\Big|_{\Gamma_{out}} = \frac{8L}{\mathrm{Re}}. \tag{25}$$

The periodical boundary conditions for velocity are applied in Γ_{in} and Γ_{out}.

$$\mathbf{u}\Big|_{\Gamma_{out}} = \mathbf{u}\Big|_{\Gamma_{in}}. \tag{26}$$

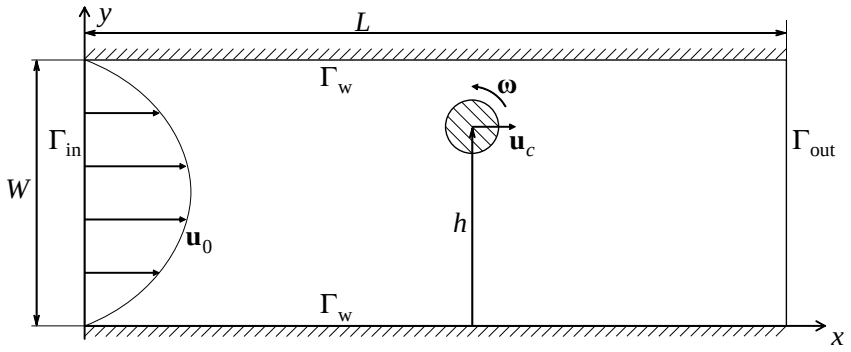

Figure 5: The scheme of the Segre-Silberberg effect simulation

When the particle approaches the outlet boundary Γ_{out}, it is relocated to the inlet boundary Γ_{in}. Note that when the particle is near Γ_{in} and Γ_{out} it influences the fluid flow of the opposite part of the fluid, as shown in the first snapshot in fig. 6. The parameters of simulation are the following: channel width $W = 1$, channel periodical length $L = 3$, particle diameter $D = 0.2$, channel Reynolds number $\mathrm{Re} = \dfrac{\rho u_0 W}{\mu} = 20$.

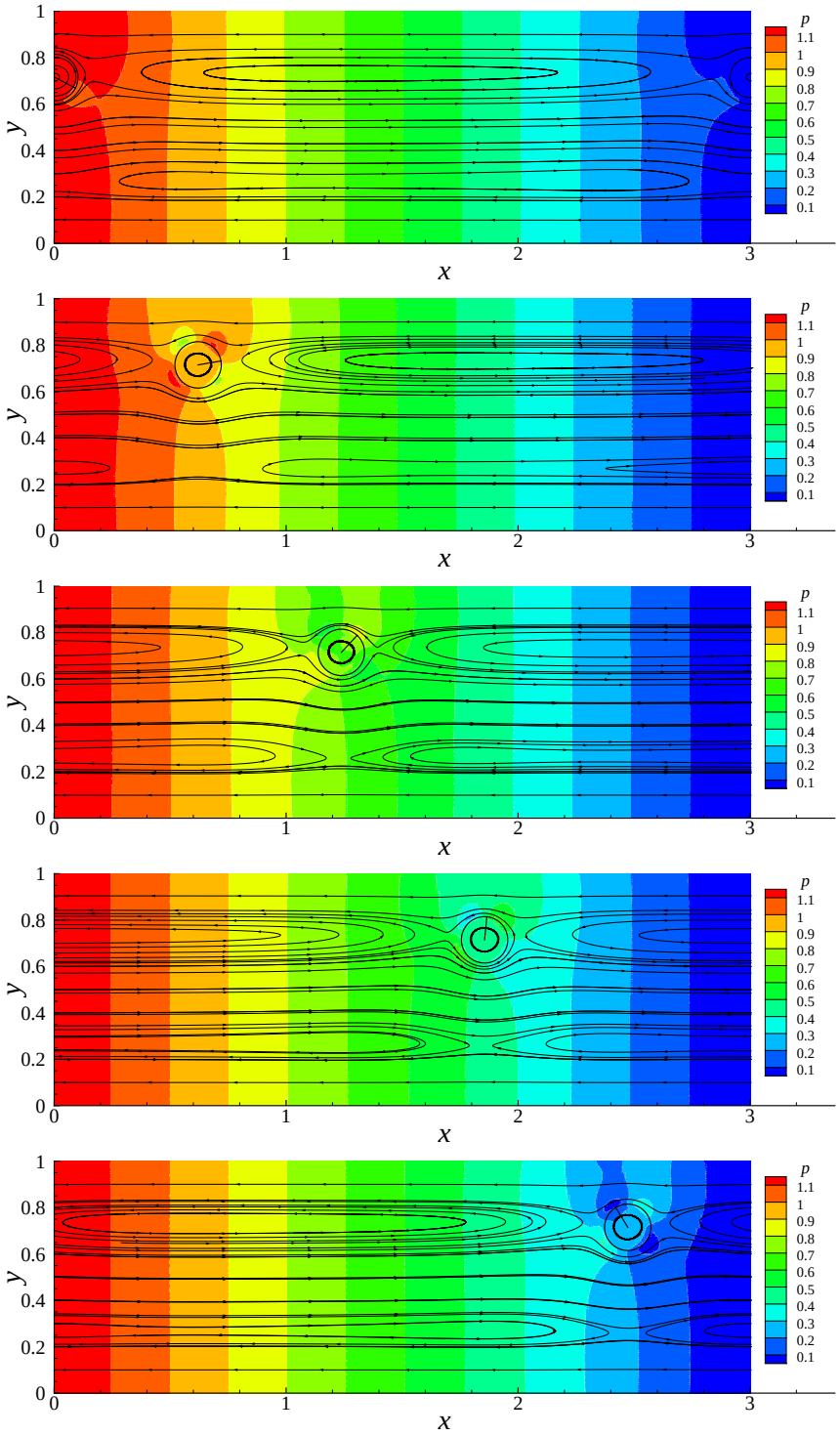

Figure 6: The particle in flat channel: snapshots of pressure distribution and streamtraces for the fluid velocity in coordinate system moving with the particle for various time moments.

In fig. 7 the velocity profiles for the undisturbed Poisseuille flow and the flow disturbed by single particle are presented. The slip velocity u_s is considerable and its value is 0.043.

The slope of the velocity profile is less in the particle than in the undisturbed flow. But near the wall the slope of the disturbed velocity is increased compared to the undisturbed flow.

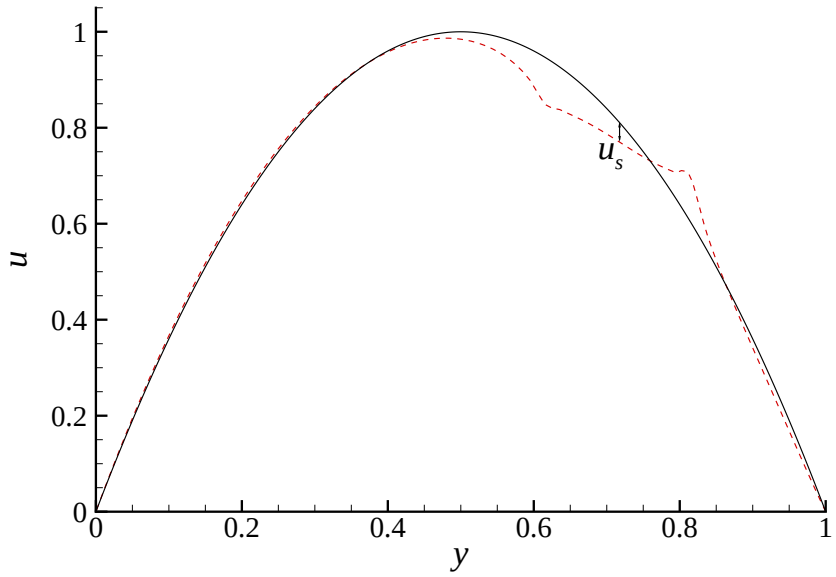

Figure 7: Velocity profile for the undisturbed Poisseuille flow (solid) and the flow disturbed by single particle (dashed).

In fig. 8 the evolution of the particle vertical position h and angular velocity is shown. The particle started from the position $h_0 = 0.51$ and migrated to the equilibrium position $h_{eq} = 0.715$. The equilibrium angular velocity equals $\omega_{eq} = 0.813$.

According to the experimental observations made in [20] and the closed-form solution [21], [22] the spherical neutrally buoyant particle placed into the Poiseuille flow occupies the position at distance $h_{eq} = 0.8$ (0.2 from the upper wall). Experimental results for two- and three-dimensional Poiseuille flow reported in [23] showed that the equilibrium positions are identical for both cases. The distance 0.2 corresponds to small particles and low Reynolds numbers. When the particle size and Reynolds number are large enough, the equilibrium position of the particle moves to the centre of the channel [24, 25], that agrees with our numerical simulations.

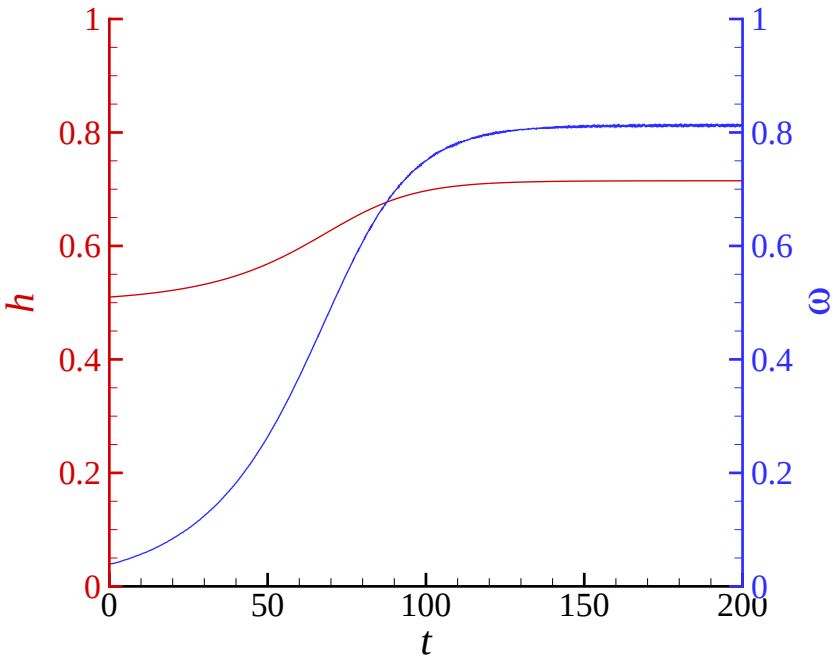

Figure 8: The particle vertical position h and angular velocity ω versus time.

5 CONCLUSION

The proposed scheme may be implemented for the simulation of disperse flows in such problems as proppant transport in hydraulic fractures, hemodynamics, separation of particles of different sizes in microflows, etc. The model was verified using benchmark problem of stationary and non-stationary overflow of cylinder in large domain, and the problem of circle particle migration in Poisseuille flow. It was shown that the method overestimates the force acting to immersed body due to the force spreading while interpolation from Lagrange grid to Eulerian grid for about 20%. The particle in the channel migrates to the equilibrium position that is closer to the center than analytically predicted.

This work is one more step to understanding the processes in disperse flows. The model is planned further to be used for simulations of many particles transport and its jamming.

ACKNOWLEDGEMENTS

The authors acknowledge the financial support of this research by the Russian Science Foundation (grant No. 17-71-20139).

REFERENCES

[1] H.H. Hu, D.D. Joseph, M.J. Crochet. Direct simulation of fluid particle motions. *Theoretical and Computational Fluid Dynamics*, 3(5):285–306, 1992.

[2] Zhi-Gang Feng, Efstathios E. Michaelides. Heat transfer in particulate flows with direct numerical simulation (dns). *International Journal of Heat and Mass Transfer*, 52(3):777 – 786, 2009.

[3] R. Glowinski, T.-W. Pan, T.I. Hesla, D.D. Joseph. A distributed lagrange multiplier/fictitious domain method for particulate flows. *International Journal of Multiphase Flow*, 25(5):755–794, 1999.

[4] R. Glowinski, T.-W. Pan, T.I. Hesla, D.D. Joseph, J. Priaux. A distributed lagrange multiplier/fictitious domain method for flows around moving rigid bodies: Application to particulate flow. *International Journal for Numerical Methods in Fluids*, 30(8):1043–1066, 1999.

[5] S. Smagulov. Fictitious domain method for the boundary problem for navier-stokes equations (in russian). *Preprint of the seminar "Methods of numerical and applied mathematics"*, (68), 1979.

[6] C.S. Peskin. Flow patterns around heart valves: A numerical method. *Journal of Computational Physics*, 10(2):252–271, 1972.

[7] Z. Hashemi, O. Abouali, G. Ahmadi. Direct numerical simulation of particle–fluid interactions: A review. *Iranian Journal of Science and Technology, Transactions of Mechanical Engineering*, 41(1):71–89, 2017.

[8] Y. Wang, A.J. Sierakowski, A. Prosperetti. Fully-resolved simulation of particulate flows with particlesfluid heat transfer. *Journal of Computational Physics*, 350:638 – 656, 2017.

[9] W.-P. Breugem. A second-order accurate immersed boundary method for fully resolved simulations of particle-laden flows. *Journal of Computational Physics*, 231(13):4469–4498, 2012.

[10] T. Kempe, J. Frhlich. Collision modelling for the interface-resolved simulation of spherical particles in viscous fluids. *Journal of Fluid Mechanics*, 709:445489, 2012.

[11] W. Fornari, A. Formenti, F. Picano, L. Brandt. The effect of particle density in turbulent channel flow laden with finite size particles in semi-dilute conditions. *Physics of Fluids*, 28(3):033301, 2016.

[12] K. Luo, Z. Wang, D. Li, J. Tan, J. Fan. Fully resolved simulations of turbulence modulation by high-inertia particles in an isotropic turbulent flow. *Physics of Fluids*, 29(11):113301, 2017.

[13] M. Uhlmann. An immersed boundary method with direct forcing for the simulation of particulate flows. *Journal of Computational Physics*, 209(2):448–476, 2005.

[14] B.E. Griffith, C.S. Peskin. On the order of accuracy of the immersed boundary method: Higher order convergence rates for sufficiently smooth problems. *Journal of Computational Physics*, 208(1):75–105, 2005.

[15] K. Luo, Z. Wang, J. Fan, K. Cen. Full-scale solutions to particle-laden flows: Multi-direct forcing and immersed boundary method. *Physical Review E*, 76(6), 2007.

[16] B. Fornberg. A numerical study of steady viscous flow past a circular cylinder. *Journal of Fluid Mechanics*, 98(04):819, 1980.

[17] D. Calhoun. A cartesian grid method for solving the two-dimensional streamfunction-vorticity equations in irregular regions. *Journal of Computational Physics*, 176(2):231–275, 2002.

[18] D. Russell, Z.J. Wang. A cartesian grid method for modeling multiple moving objects in 2d incompressible viscous flow. *Journal of Computational Physics*, 191(1):177–205, 2003.

[19] S. Xu, Z.J. Wang. An immersed interface method for simulating the interaction of a fluid with moving boundaries. *Journal of Computational Physics*, 216(2):454–493, 2006.

[20] G. Segr, A. Silberberg. Behaviour of macroscopic rigid spheres in poiseuille flow part 2. experimental results and interpretation. *Journal of Fluid Mechanics*, 14(1):136157, 1962.

[21] B. P. Ho, L. G. Leal. Inertial migration of rigid spheres in two-dimensional unidirectional flows. *Journal of Fluid Mechanics*, 65(2):365400, 1974.

[22] P. Vasseur, R.G. Cox. The lateral migration of a spherical particle in two-dimensional shear flows. *Journal of Fluid Mechanics*, 78(02):385, 1976.

[23] M. Tachibana. On the behaviour of a sphere in the laminar tube flows. *Rheologica Acta*, 12(1):58–69, 1973.

[24] E.S. Asmolov, A.L. Dubov, T.V. Nizkaya, J. Harting, O.I. Vinogradova. Inertial focusing of finite-size particles in microchannels. *Journal of Fluid Mechanics*, 840:613–630, 2018.

[25] J. Feng, H.H. Hu, D.D. Joseph. Direct simulation of initial value problems for the motion of solid bodies in a newtonian fluid. part 2. couette and poiseuille flows. *Journal of Fluid Mechanics*, 277(1):271, 1994.